Planetary and Space Science 170 (2019) 29–41

Contents lists available at ScienceDirect

Planetary and Space Science

journal homepage: www.elsevier.com/locate/pss

# The upper atmosphere of Venus: Model predictions for mass spectrometry measurements

S. Gruchola *, A. Galli, A. Vorburger, P. Wurz

*Physikalisches Institut, University of Bern, Sidlerstrasse 5, 3012, Bern, Switzerland*

ARTICLE INFO

*Keywords:*
Venus
Atmosphere
Density profiles
Mass spectra
Noble gases

ABSTRACT

Venus is the closest and most similar planet to Earth in the whole solar system, yet, basic measurements are missing. The atmospheric composition has been studied to some extent with the Pioneer Venus Orbiter mission and the more recent Venus Express, however, the concentration of many species and their isotopic ratios are not yet known with satisfying accuracy. Especially when it comes to the heavy noble gases as Kr and Xe, there is little to no collected data in this field. These elements form a key link to the reconstruction of the atmospheric evolution, which would deliver crucial information on the formation of Earth-like bodies. Knowing the abundances of the noble gases may allow us to answer the question why Venus did not evolve to a potentially habitable planet like its neighbour Earth.

This paper presents a meta-study of existing observations of Venus' upper atmosphere and exosphere and an exospheric model of the thermal and hot atmosphere of Venus above the homopause. Mass spectra for possible future Venus missions are predicted, as for example the EnVision mission of ESA. The main focus are the heavy noble gases and requirements for the trajectories are proposed. In addition, mass spectra and recommended integration times for the Venus flyby of ESA's JUICE mission are derived.

## 1. Introduction

Venus with its radius and mass comparable to Earth is far from being habitable. The atmosphere consists almost exclusively of carbon dioxide, the pressure is at present ninety times that on Earth and the surface temperature exceeds 730 K (Williams, 2016).

In the past, there have been several missions to explore our closest neighbour. The first successful one was the Mariner 2 mission in 1962. Mariner 2 confirmed the hot temperature near the surface and observed a much colder one at the cloud top. It also measured the intrinsic magnetic field of Venus to be almost non-existent. As a consequence, Venus' exosphere is in direct interaction with the solar wind, which affects the loss rate of light elements (Bailey, 2013).

After several more Mariner missions conducted by the United States and Venera missions by the Soviet Union, which studied the surface composition by landing on the planet (Basilevsky et al., 2007), the Pioneer Venus launched in 1978. The project consisted of two separate spacecraft, an orbiter (Pioneer Venus 1) and a multiprobe (Pioneer Venus 2). Among other things, experiments to study the atmospheric composition, the clouds and the surface were conducted. Pioneer Venus observed the thermosphere to be much colder than the mesosphere below it, at around 100 K. It also measured the temperature gradient from the day-to the nightside and discovered an accumulation of light species such as H and He at the terminator (Colin and Hall, 1977).

In 1989, the Magellan mission was launched by NASA and it delivered important information about the geology and geophysics of Venus. Using radar imaging, Magellan mapped 95 % of the planet's surface and studied the volcanic landforms. High-resolution gravity data was collected by two-way Doppler tracking of the spacecraft, which was aided by an aerobraking maneuver to lower the satellite's orbit from a highly elliptical orbit to a near-circular one (Bindschadler, 1995).

More recently, in 2005, ESA sent out Venus Express. Among other things, the mission gathered data on the atmospheric structure and dynamics, the composition and chemistry, the cloud layers and hazes as well as atmospheric escape processes. The science payload consisted of seven instruments, among which were the UV-IR spectrometers SPICAV and SOIR, as well as the UV-VIS-IR spectrometer VIRTIS (Svedhem et al., 2009).

The latest orbiter mission sent to Venus was Akatsuki, conducted by JAXA and launched in 2010. The spacecraft was designed to study the climate and meteorology of the Venusian atmosphere. With a longwave infrared camera, the spacecraft collected data of the brightness

* Corresponding author.
*E-mail address:* salome.gruchola@space.unibe.ch (S. Gruchola).

https://doi.org/10.1016/j.pss.2019.03.006
Received 7 September 2018; Received in revised form 16 January 2019; Accepted 12 March 2019
Available online 17 March 2019

temperature distribution and like Venus Express, retrieved the wind-vector field at the cloud-top using a cloud tracking technique (Taguchi et al., 2012).

Despite all those previous missions to study Venus, basic measurements are still missing. One of the most prominent one is the concentration of the heavy noble gases in the atmosphere. Noble gases are not involved in any chemical reactions, and given that their mass is large enough to prevent them from getting carried away from the atmosphere of the planet, their concentration is not decreasing with time. On the contrary, because these noble gases can be produced below the surface and released into the atmosphere through volcanism, for which signs of recent or current activity exist (Taylor et al., 2018), more and more noble gases are accumulated. Measuring the abundance of the heavy noble gases today could give us valuable information on how long Venus has been in its present state and what it was like before. In addition, this would provide us with important information about the evolution of terrestrial planets in general, since Earth, in contrast to Venus, is belived to have suffered a collision with a planetesimal, which led to the formation of the Moon and the loss of a large amount of atmospheric gases (Donahue and Russel, 1997). This is a further reason why future missions to Venus are already planned by several space agencies, for example the EnVision project by ESA (Ghail et al., 2018).

This paper presents an exospheric model of Venus' upper atmosphere. In contrast to other models as for example the Venus International Reference Atmosphere (VIRA) (Keating et al., 1985; Vandaele et al., 2016), density profiles of less abundant species were computed, in total 22 thermal species and 4 hot species, and photochemical dissociation was included in the model. Mass spectra of the thermal and hot species at various altitudes will be presented, which are relevant for future Venus orbital missions. The paper puts a focus on the heavy noble gases krypton and xenon.

The exospheric model used to model the upper atmosphere was derived by adapting an existing exospheric code to Venus. The code has previously been used to model the atmospheres of other planets and bodies (Wurz and Lammer, 2003; Wurz et al., 2007; Vorburger et al., 2015b). There are many atmospheric codes which contribute to model the atmosphere of Venus, including the Global Circulation Models. Emphasising that our code cannot model the thick layers of the lower atmosphere, it predicts density profiles at higher altitudes which is necessary to interpret UV line observations and in-situ measurements. A satellite is not able to orbit Venus below the homopause, therefore, we need to know more about the region above to predict where we will get in-situ mass spectrometer data.

## 2. Method

### 2.1. Model description

The simulation package used to obtain the models of the Venus atmosphere is based on a Monte Carlo Simulation originally developed for Mercury and the Moon (Wurz and Lammer, 2003; Wurz et al., 2007). The program is therefore, strictly speaking, only applicable to the atmospheric region, where collisions are negligible, namely the exosphere. In this region, the mean free path is longer than the scale height. The simulations should start at the exobase, which is located at around 210 km on the dayside and sinks to around 154 km on the nightside because of the IR emission from the $CO_2$ atmosphere (Kasprzak et al., 1997). The difference between the exobase levels comes from the heating by the Sun, which heats up the dayside thermosphere, resulting in larger scale heights. Unfortunately, choosing the exobase as the altitude level, from where the simulations are conducted had to be rejected for Venus. This will be discussed in more detail in Section 2.3.

The program starts with one particle and then assigns to it a random direction and a random initial velocity chosen from a prescribed distribution, which depends on the most probable velocity. According to the Maxwell Boltzmann distribution, the mean velocity is given by

$$\left\langle \nu \right\rangle = \sqrt{\frac{8\, k_B\, T}{\pi\, m}}, \tag{1}$$

and therefore depends on the temperature, $T$, at the location where the particles are released. In Equation (1), $k_B$ stands for the Boltzmann constant and $m$ is the mass of the particle.

Given the velocity and direction of the particle, the program numerically computes the trajectory of the particle using discrete steps. The same approach has already been used to compute Callisto's exosphere (Vorburger et al., 2015b), as well as for the exospheres of Mercury and the Moon (Wurz and Lammer, 2003; Wurz et al., 2007). The density of the gas at a given altitude is related to the time a particle at this altitude needs to get to the next step on the trajectory. The longer this time, the higher the density. The program then repeats this process for a given number of particles. The larger this number of initial particles, the smaller the statistical uncertainties of the trajectory.

Most species in the Venusian exosphere can be understood as a two-temperature particle distribution, with a thermal and hot component. For the thermal component, $T$ equals the temperature of the thermosphere, which implies that the typical velocity of a particle is determined by the temperature of the atmosphere around it. The particles forming the hot component have much higher energies and therefore higher velocities. In our program, the hot atmosphere has been simulated the same way as the thermal one with the only difference being a much higher initial temperature $T$, which results in higher velocities of the particles, according to Equation (1). The hot components are mainly produced by the dissociative recombination of ions near the exobase (Keating et al., 1985). Another source of hot particles is photochemical dissociation, which is caused by solar ultraviolet radiation breaking up molecules in the atmosphere (Bertaux et al., 2007). In our model, photochemical dissociation is computed by comparing the time the particles spend at a certain height to the theoretical dissociation time. If photochemical dissociation does happen, based on Poisson statistics, the released binding energy gets distributed onto the fragments according to their mass which results in large velocities. Then, the trajectories of the fragments are calculated the same way as the ones of the parent molecules, using the assigned velocities. A more detailed description of the photochemical dissociation can be found in Appendix A.

Photochemical dissociation plays a major role in escape processes if it happens above the exobase. Below, collisions prevent the fragments and ions from escaping the atmosphere. In the exospheric model presented in this paper, collisions as well as other processes which take place above the homopause as e.g. sputtering, charge exchange or photolysis are not addressed. However, this paper focusses on the noble gases which do not undergo photochemical dissociation and have a lower cross section for ionisation and charge exchange than non-noble gases. Also, the abundance of the heavy noble gases Kr and Xe at the exobase is negligible, as will be shown in Section 3, sputtering is therefore not relevant. The uncertainty in the abundance of those noble gases at the homopause is much greater than the model's deviation from the actual conditions due to the processes mentioned before.

### 2.2. Total number density of the atmosphere

The lower atmosphere of Venus is composed mostly of $CO_2$ and $N_2$ with an abundance of 96.5 % and 3.5 %, respectively (see review by de Pater and Lissauer, 2001). Assuming all gases to be ideal and taking into account the dominance of $CO_2$, the total number density of the lower atmosphere is related to the $CO_2$ density by

$$n = \frac{n_{CO_2}}{0.965}. \tag{2}$$

The latest measurements of $CO_2$ in the atmosphere of Venus were conducted with the SOIR spectrometer on board the ESA Venus Express mission (Mahieux et al., 2012). The densities of $CO_2$, which are of

**Table 1**
$CO_2$ abundances and temperatures, retrieved from Mahieux et al. (2012). The values correspond to an equatorial measurement (orbit 1567.1) at the Venus terminators. The error ranges between 1 and 5 %.

| Altitude [km] | Number density [$m^{-3}$] | Estimated error | Temperature [K] | Estimated error | References |
|---|---|---|---|---|---|
| 100 | $10^{21}$ | 1–5% | 184 | 1–20 K | [1] |
| 120 | $10^{19}$ | 1–5% | 176 | 1–20 K | [1] |

[1]Mahieux et al. (2012).

interest in this paper, are summarised in Table 1, together with the corresponding temperatures. Measurements were performed at the Venus terminators, whereas the models in this paper were computed at the equator at noon. The discrepancies between model and the observations which might result from using terminator temperatures were accepted because of the lack of more accurate data.

The mixing ratio of the $i^{th}$ species can now be defined as the ratio of its number density $n_i$ and the total number density $n$ (von Zahn et al., 1983), namely

$$x_i = \frac{n_i}{n}. \tag{3}$$

### 2.3. Homopause level

As our exospheric model is based upon a Monte Carlo Simulation, a boundary condition, namely the abundance of the species at the exobase, is required. However, most data on the abundance of the various species, especially the heavy ones, are only present in terms of mixing ratios, which are solely valid below the homopause. There, the atmosphere is assumed to be mixed homogeneously. The boundary had therefore to be chosen much lower within the homosphere. Since collisions should not be neglected in this part of the atmosphere, slight discrepancies between our model and actual observations may occur.

It came not without difficulties to choose the appropriate boundary altitude from which the collisionless particle trajectories would be computed. At first sight the best option might seem to choose the homopause as initial altitude. It is indeed much lower than the exobase, but the species tend to separate according to the Boltzmann distribution above, just as in the exosphere. Above the homopause, the pressure $p$ at an altitude $z$ is therefore given by

$$p(z) = p_0 \exp\left(-\frac{m\,g}{k_B T} z\right) = p_0 \exp\left(-\frac{z}{H}\right). \tag{4}$$

In Equation (4) above, the scale height $H$ has been introduced,

$$H = \frac{k_B T}{m\,g}, \tag{5}$$

which is defined as the height after which the pressure decreases by a factor $e \approx 2.72$. The heavier the species, i.e., the bigger the molecular mass $m$, the smaller the scale height. This leads to a vertical fractionation of the gases above the homopause according to their mass, and to mixing ratios which are no longer constant. Usually, the scale height $H$ is not a constant due to the altitude dependence of the gravitational acceleration $g(z)$ and the temperature $T(z)$. Moreover, the mean molecular mass of the atmosphere is altitude dependent above the homopause.

Choosing the homopause level as initial altitude entails the difficulty that it is not a sharp boundary but more an altitude range. From the most recent carbon dioxide measurements in the Venus mesosphere by SOIR on board the ESA Venus Express, a homopause level between 124 and 134 km has been derived (Mahieux et al., 2012). This is consistent with de Pater and Lissauer (2001), who located the homopause in the range of 120–132 km. There are two more problems: First, the homopause is species dependent (von Zahn et al., 1983) which implies that it is situated lower for heavier species than for the lighter ones. And second, the homosphere cannot be assumed to be mixed homogeneously, seeing that it contains a sulfuric and chemically active cloud region between 48 and 68 km which separates the lower atmosphere from the upper one (Donahue and Russel, 1997).

Using mixing ratios immediately relates the number densities of all species with the $CO_2$ density, according to Equations (3) and (2). $CO_2$ with a molecular mass of 44 u is rather heavy, therefore, it's homopause is probably lower than the one of light species. Choosing the boundary level too high, i.e., at an altitude, where the mixing is no longer homogeneous, leads to an underestimation of the number densities of species lighter than $CO_2$. They show a slower decrease due to their larger scale height, whereas heavier species would have already decreased by a larger factor and would therefore be overestimated. Choosing it too low leads to difficulties as well. This leads to the assumption that the species separate proportionally to their mass at lower altitudes than in reality. This would cause an overestimation of light species and an underestimation of ones heavier than $CO_2$.

Addressing all concerns, we chose to set the boundary for species heavier than $CO_2$, for all sulfur compounds and for species which have only been measured in the lower atmosphere to 100 km. For all others, we set it to 120 km, which is the lower limit given by de Pater and Lissauer (2001).

It must be taken into consideration, that the small scale heights of heavy species result in vast differences in the density profiles depending on the boundary altitude. This has also a large impact on the region in which the species are detectable by mass spectrometers on board a satellite. This will be further discussed in Section 3.2.

### 2.4. Input parameters

#### 2.4.1. Abundances of thermal components

In this section, the abundances of the modelled species which were

**Table 2**
Used abundances of thermal atoms below Venus' homopause.

| Species | $M_{mol}$ [u] | Abundance | Estimated error | $H_{start}$[km] | T [K] | Altitude range | References |
|---|---|---|---|---|---|---|---|
| H | 1.0079 | $2 \cdot 10^{11}$ $m^{-3}$ | $\pm 1 \cdot 10^{11}$ $m^{-3}$ | 255 | 320 | @ 255 km | [1] |
| He | 4.0026 | 4 ppm | $^{+34}_{-1}$ ppm | 120 | 176 | 120–130 km | [2], [3] |
| C | 12.0107 | 0.00965% | not available | 120 | 176 | 120–250 km | [1] |
| N | 14.0067 | 0.0145% | not available | 120 | 176 | 120–150 km | [2],[4] |
| O | 15.9994 | 0.965% | not available | 120 | 176 | 95–120 km | [5],[6],[7],[8] |
| Ne | 20.1797 | 7 ppm | ±3 ppm | 120 | 176 | 0–120 km | [9] |
| Ar | 39.948 | 30 ppm | 33 % | 100 | 184 | lower atmosphere | [10],[12] |
| Kr | 83.898 | $\leq$ 69 ppb | 1 order of magnitude | 100 | 184 | lower atmosphere | [10],[11] |
| Xe | 131.293 | $\leq$ 0.10 ppm | 1 order of magnitude | 100 | 184 | lower atmosphere | [10],[11] |

[1]Keating et al. (1985), [2]von Zahn and Moroz (1985), [3]Krasnopolsky and Gladstone (2002), [4]Kasprzak et al. (1980), [5]Gérard et al. (2009), [6]Von Zahn et al. (1980), [7]Keating (1980), [8]Hedin et al. (1983), [9]von Zahn et al. (1983), [10]Donahue et al. (1981), [11]Chassefière et al. (2012), [12]Taylor (2014).

used as input parameters for the Monte Carlo Simulation are summarised. The values can be found in Tables 2 and 3, together with their molecular mass $M_{mol}$ and the starting altitude for the simulation $H_{start}$. We shall now have a closer look at the validity of the abundances assumed for the model, starting with the atomic components of the atmosphere.

*Hydrogen (H):*

Lyman-$\alpha$ airglow observations of the hydrogen corona have been conducted by several Venera and Mariner missions, the Pioneer Venus Orbiter and more recently with SPICAV on board Venus Express (von Zahn and Moroz, 1985; Chaufray et al., 2012). The data obtained yielded two different scale heights which was interpreted by Anderson (1976) as the result of two hydrogen populations, a hot and thermal one, with different temperatures. The thermal hydrogen density obtained by Mariner 5 at 255 km was $n_H = (2 \pm 1) \cdot 10^{11}$ m$^{-3}$ at a temperature of 275 ± 50 K (Keating et al., 1985). SPICAV on board the ESA Venus Express measured a thermal hydrogen number density of $n_H = 1.217 \cdot 10^{11}$ m$^{-3}$ at 250 km altitude on the dayside (Chaufray et al., 2012). The value used in this paper is $n_H = 2 \cdot 10^{11}$ m$^{-3}$, and extrapolation was applied to obtain the densities below 255 km, which were required for the mass spectra. The temperature of the atmosphere was derived from interpolation of the data found by the SOIR spectrometer on board Venus Express (Mahieux et al., 2012).

*Helium (He):*

The mixing ratio of helium is assumed to be around 12 ppm (de Pater and Lissauer, 2001) or between 4 and 36 ppm (von Zahn and Moroz, 1985), however these densities were extrapolated to the lower atmosphere. The lowest in situ measurements were reported from the Pioneer Venus Bus Neutral Mass Spectrometer (PV-BNMS) at 130 km and yielded a mixing ratio of $\frac{n_{He}}{n_{CO_2}} = 4.9 \cdot 10^{-5}$ (Von Zahn et al., 1980). The simulation has been conducted with mixing ratios of 4 ppm, 12 ppm and 36 ppm at 120 km, however the results obtained from a mixing ratio of 4 ppm agreed best (see Section 3) with observational data obtained by PV-BNMS (Von Zahn et al., 1980). A further reason why using the lower limit for the helium abundance to simulate the dayside atmosphere seems reasonable, is that strong winds across the terminator carry gases which are lighter than $CO_2$ to the nightside, leading to buldges at the terminators and a lower helium density on the dayside (Niemann et al., 1980). Furthermore, choosing 4 ppm is consistent with the mixing ratio of 9 ± 6 ppm, derived from the most recent long-exposure spectroscopy measurements with the Extreme Ultraviolet Explorer (EUVE) and accounting for the uncertainty associated with eddy diffusion (Krasnopolsky and Gladstone, 2002).

*Carbon (C):*

No measurements of atomic carbon have been conducted so far. Keating et al. (1985) make use of the ratio of the abundance of $O_2$ and $CO_2$ to estimate the carbon density. Additionally, they use the measurements of hot carbon by the Pioneer Venus Orbiter Ultraviolet Spectrometer (PV-OUVS) to conclude that a thermal carbon abundance of $n_C = 0.01 \cdot n_O$ at the exobase at 250 km is required to explain the observed hot $C^+$ densities (Keating et al., 1985). In the current simulations, the same ratio has been used at 120 km, taking into account the similar molecular masses of carbon and oxygen and their therefore similar scale heights.

*Nitrogen (N):*

Atomic nitrogen was first measured by the Pioneer Venus Orbiter Neutral Mass Spectrometer (PV-ONMS) in the thermosphere (Kasprzak et al., 1980; von Zahn and Moroz, 1985). It was found that there exists a close proportionality between the densities of atomic nitrogen and oxygen, with an average value of $\frac{n_N}{n_O} = 0.015$ at 150 km altitude (Kasprzak et al., 1980; von Zahn and Moroz, 1985). Taking into account the small mass difference between the two species, the same ratio has been assumed at 120 km.

*Oxygen (O):*

Atomic oxygen gets produced on the dayside by $CO_2$ photolysis and ion-neutral chemical reactions and is then transported to the nightside by the global wind system (Brecht et al., 2012). The mixing ratio of atomic oxygen and carbon dioxide increases rapidly above 135 km, reaching a value of around 4 at 170 km (von Zahn and Moroz, 1985). From measurements made by the PV-ONMS, Von Zahn et al. (1980), Keating (1980), and Hedin et al. (1983) derived ratios of $\frac{n_O}{n_{CO_2}}$ of 0.17, 0.15 − 0.18, and 0.20, respectively, at 140 km. Comparing results from our simulation model with the measurements and the modelled ratios mentioned above, the density of atomic oxygen at 120 km has been set to $n_O = 0.01 \cdot n_{CO_2}$ which corresponds to $1 \cdot 10^{17}$ m$^{-3}$. Assuming the ratio to be smaller at 120 km than at 140 km is in agreement with the larger scale height of oxygen compared to $CO_2$.

More recent, Gérard et al. (2009) derived O densities from the $O_2$ IR nightglow observations with a maximum between $1 \cdot 10^{17}$ and $5 \cdot 10^{17}$ m$^{-3}$ at an altitude ranging from 95 to 115 km (Gérard et al., 2009). Brecht et al. (2012) modelled the oxygen atom density using a Venus Thermospheric General Circulation Model (VTGCM) and derived a maximum density value of $3.41 \cdot 10^{17}$ m$^{-3}$ at 104 km at the equator at midnight. The VTGCM model without trace species yielded an oxygen

**Table 3**
Used abundances of thermal molecules below Venus' homopause.

| Species | $M_{mol}$ [u] | Abundance | Estimated error | $H_{start}$[km] | T [K] | Altitude range | Refrences |
|---|---|---|---|---|---|---|---|
| $H_2$ | 2.016 | 1 ppb | not available | 120 | 176 | @ 120 km | [1] |
| $NH_3$ | 17.031 | 1 ppb | not available | 120 | 176 | @ 120 km | [2],[3] |
| $H_2O$ | 18.015 | 0.8 ppm | $^{+1.2}_{-0.5}$ ppm | 120 | 176 | mesosphere | [4],[5],[6] |
| HF | 20.006 | 2 ppb | ± 1 ppb | 120 | 176 | mesosphere | [4],[5] |
| CO | 28.0101 | ≤ 40000 ppm | $^{+0}_{-39300}$ ppm | 120 | 176 | @120 km | [7] |
| $N_2$ | 28.0134 | 3.5% | ± 0.8 % | 120 | 176 | 0–120 km | [4],[8] |
| $O_2$ | 31.9988 | 8.6 ppm | $^{+11.4}_{-8.6}$ ppm | 120 | 176 | @120 km | [4],[9] |
| $H_2S$ | 34.0809 | ≤ 1 ppb | not available | 100 | 184 | @100 km | [10] |
| HCl | 36.4609 | 0.1 ppm | ± 0.03 ppm | 120 | 176 | 70–75 km | [4],[11] |
| $CO_2$ | 44.0095 | 96.5% | 1 − 5% | 120 | 176 | 0–120 km | [12] |
| $SO_2$ | 64.0638 | 0.1 ppm | $^{+0.1}_{-0}$ ppm | 100 | 184 | 75–110 km | [9],[13] |
| COS | 90.9982 | ≤ 1 ppb | not available | 100 | 184 | @100 km | [9] |
| $H_2SO_4$ | 98.0785 | 1 ppb | $^{+0}_{-0.9}$ ppb | 100 | 184 | @100 km | [14] |

[1]Krasnopolsky and Gladstone (2002), [2]Owen and Sagan (1972), [3]Krasnopolsky (2012), [4]de Pater and Lissauer (2001), [5]Bertaux et al. (2007), [6]Cottini et al. (2012), [7]Vandaele et al. (2016), [8]von Zahn et al. (1983), [9]Krasnopolsky (2010), [10]Krasnopolsky (2008), [11]Bertaux et al. (2007), [12]Mahieux et al. (2012), [13]Marcq et al. (2013), [14]Zhang et al. (2010).

density of around $3 \cdot 10^{16}$ $m^{-3}$ at 120 km at the same geographical location. This value is smaller by approximately a factor 3 than the oxygen density chosen in our model which seems legitimate given that the oxygen density is higher on the dayside (Brecht et al., 2012).

*Neon (Ne):*

Neon has a mixing ratio of 7 ppm (von Zahn et al., 1983; de Pater and Lissauer, 2001) with an error of ±3 (von Zahn et al., 1983). Taylor et al. (2018) assume a similar value of 5 ppm. Measurements of Ne have only been performed in the lower atmosphere by Venera 11 and 12 mass spectrometers (von Zahn et al., 1983), however, a constant mixing ratio is assumed up to the homopause at 120 km due to the fact that noble gases are not reactive and therefore not involved in chemical reactions taking place in the atmosphere. In addition, neon with a chemical mass of 20.1797 u is rather light compared to other noble gases as krypton and xenon.

*Argon (Ar):*

The mixing ratio of Ar was measured by the PV-BNMS in the lower atmosphere and a value of 70 ppm was obtained (von Zahn et al., 1983; de Pater and Lissauer, 2001; Taylor et al., 2018). von Zahn et al. (1983) additionally mention an uncertainty of ± 25 ppm. However, these values were measured at around 20 km, far below the assumed homopause level. Donahue et al. (1981) estimate a mixing ratio of around 30 ppm, which has also been used in the current simulation, together with a homopause level of 100 km, seeing that measurements are only available far below the homopause level. Taylor (2014) mentions an abundance of 31 ppm together with an uncertainty of 33 %.

*Krypton (Kr):*

According to Chassefière et al. (2012), the krypton abundance has an uncertainty of one order of magnitude. Krypton was first measured by Venera 11 and 12 mass spectrometers (von Zahn et al., 1983). and Istomin et al. (1980) reported a mixing ratio of $^{84}Kr$ of about 0.5 ppm. Hoffman et al. (1980a) estimated a Kr mixing ratio of 0.2 ppm from the measurements of the Pioneer Venus Large Probe Neutral Mass Spectrometer (PV-LNMS) (von Zahn et al., 1983), whereas Donahue et al. (1981) assumed the most probable mixing ratio to be around 47 ppb with an upper limit of 69 ppb. For this work, the upper limit of 69 ppb was chosen as an optimistic value for the abundance, together with a homopause level of 100 km.

*Xenon (Xe):*

Xenon has not been measured in the Venusian atmosphere so far, hence, no direct data exist (von Zahn et al., 1983). Based on the mixing ratios of Ar and Kr, Donahue et al. (1981) derived an upper limit of around 0.12 ppm for the Xe mixing ratio. de Pater and Lissauer (2001) propose the same mixing ratio. The most optimistic case would be to have said mixing ratio at altitudes of 130 km or higher. However, taking into consideration the large chemical mass of xenon of 131.293 u, it seems more likely that the xenon abundance starts dropping much earlier according to the exospheric model. Hence, the value used for the simulations is 0.1 ppm, together with a homopause level at 100 km. However, Donahue et al. (1981) assume that there is probably considerably less Xe in the atmosphere of Venus and they propose an upper limit of only around 40 ppb. As for krypton, the abundance of xenon has, according to Chassefière et al. (2012), an uncertainty of one order of magnitude, the worst case would therefore come true if the mixing ratio doesn't exceed 10 ppb.

Having introduced the most important thermal atomic species present in the atmosphere of Venus, we proceed to the molecular ones, starting with the hydrogen molecule $H_2$.

*Hydrogen molecule (H2):*

Krasnopolsky (2010) reports a $H_2$ mixing ratio of 4 ppb at 47 km. Due to its long chemical lifetime, he assumed the abundance to be the same at 80 km. In our model, the mixing ratio of $H_2$ at 120 km was assumed to be around 1 ppb by taking into account the long chemical lifetime and the small molecular mass, which also leads to a large scale height.

*Ammonia (NH3):*

Ammonia was first measured by the Venera 8 lander at altitudes of 44 and 32 km (von Zahn et al., 1983). From these measurements, Surkov et al. (1974) estimated a mixing ratio of $NH_3$ in the range of $10^{-3}$ and $10^{-4}$. However, Young (1977) pointed out that the Venera 8 detector could not distinguish $NH_3$ from $H_2SO_4$, which is the principal constituent of the cloud layers (Donahue and Russel, 1997), thus, the ammonia abundance is probably much lower than reported by Venera 8. Neither the PV-LNMS nor the Venera 11 and 12 missions detected any ammonia (von Zahn et al., 1983), but an upper limit of $1 \cdot 10^{-7}$ for the $NH_3$ mixing ratio was obtained from Earth-based spectroscopy observations by Owen and Sagan (1972), valid at the cloud tops (von Zahn et al., 1983). Krasnopolsky (2012) report a $NH_3$ $2\sigma$ upper limit mixing ratio of 6 ppb above the cloud tops from observations at NASA IRTF, while pointing out that it quickly dissociates in the mesosphere. Hence, in the time $NH_3$ molecules need to reach 120 km some of them dissociate and the abundance at this altitude is therefore presumably lower. In our model a mixing ratio of 1 ppb at 120 km was assumed.

*Water (H2O):*

de Pater and Lissauer (2001) report a water vapour mixing ratio of 0.8 ppm, valid in the mesosphere, which extends up to 120 km (de Pater and Lissauer, 2001). Water has also been measured by SOIR on board VEX and values between 0.3 and 1 ppm were reported with no decrease up to altitudes of around 110 km, where measurements were conducted (Bertaux et al., 2007). This has been interpreted to be caused by local condensation. The Visible and Infrared Thermal Imaging Spectrometer (VIRTIS) aboard VEX measured a water mixing ratio from 0.5 to 2 ppm in the altitude range between 75 and 110 km (Cottini et al., 2012). Therefore, in this work the mixing ratio of 0.8 ppm given by de Pater and Lissauer (2001), which lies in the range given by Bertaux et al. (2007) and Cottini et al. (2012), has been adopted at 120 km.

*Hydrogen fluoride (HF):*

The mixing ratio of HF given by de Pater and Lissauer (2001) is 2 ppb in the mesosphere, whereas Taylor et al. (2018) assume 5 ppb. HF was first identified by the Earth-based observations conducted by Connes et al. (1967) with an abundance ratio $n_{HF} = 5 \cdot 10^{-9}\, n_{CO_2}$, at around 64 km. SOIR on board the ESA Venus Express measured a value in the range of 1–3 ppb at altitudes 75–85 km (Bertaux et al., 2007). Since the data for the simulation was required at a much higher altitude of 120 km, the smaller value of 2 ppb from de Pater and Lissauer (2001) and mean value of the most recent measurements by Bertaux et al. (2007) was chosen.

*Carbon monoxide (CO):*

CO is produced in the mesosphere by dissociation of $CO_2$ by solar ultraviolet radiation (Taylor et al., 2018), and circulations of the atmosphere transport the products CO and O to the nightside (Vandaele et al., 2015), resulting in strong variations of the CO density. de Pater and Lissauer (2001) estimate a lower limit of 200 ppm in the mesosphere, von Zahn et al. (1983) recommend a mixing ratio in the range of 350–1400 ppm and from SOIR aboard VEX the CO density at 120 km is assumed to lie between 700 and 40000 ppm, with a mean value around 3300 ppm (Vandaele et al., 2016). Additionally, SOIR recorded an enormous increase of the order of $10^4$ from 70 km up to 140 km (Vandaele et al., 2016). The ranges encompass the strong diurnal variations. VIRTIS aboard VEX measured a CO number density of the order of $10^{17}$ $m^{-3}$ at 120 km at the equator at a local solar time between 10 and 14 h, which corresponds to a mixing ratio of 10000 ppm (Gilli et al., 2015). For the simulations, the upper limit of 40000 ppm given by Vandaele et al. (2016) was used, seeing that these results agreed most with the observational data obtained from the PV-ONMS (Kasprzak et al., 1980). It furthermore seems legitimate to use the upper limit for the simulations since they are conducted on the dayside where the solar ultraviolet radiation is at its strongest and therefore the production rate of CO is at its highest.

*Nitrogen molecule (N2):*

$N_2$ is the second most common species in the atmosphere of Venus,

right after $CO_2$, with an abundance of 3.5 % (de Pater and Lissauer, 2001; von Zahn et al., 1983). von Zahn et al. (1983) state an uncertainty of ± 0.8 %. $N_2$ has been measured by the PV-BNMS and at 150 km a number density of $n_{N_2} = 1.1 \cdot 10^{15}$ m$^{-3}$ has been obtained (Von Zahn et al., 1980). Von Zahn et al. (1980) also mention a homopause altitude of 136 km for $N_2$.

*Oxygen molecule (O2):*

The abundance of $O_2$ in the atmosphere of Venus is, unfortunately, poorly established and no in-situ measurements have been conducted above the cloud top so far. de Pater and Lissauer (2001) estimate a mixing ratio between 0 and 20 ppm in the lower atmosphere, and Gelman et al. (1979) derived 20 ppm as an upper limit anywhere below 42 km. From observations with a high-resolution long-slit spectrograph CSHELL at the NASA Infrared Telescope Facility (IRTF) on Mauna Kea, Hawaii, Krasnopolsky (2010) calculated a mixing ratio of 5–8.6 ppm at 80 km. As no data are available at higher altitudes, the upper limit of 8.6 ppm, given by Krasnopolsky (2010), was adopted in this paper at 120 km.

*Hydrogen sulfide (H2S):*

According to von Zahn et al. (1983), hydrogen sulfide is produced in the lower atmosphere and is then destructed in the clouds due to chemical reactions. In the lower atmosphere, the PV-LNMS measured a $H_2S$ mixing ratio of 3 ± 2 ppm below 20 km (Hoffman et al., 1980a), and from data obtained by the Large Probe Gas Chromatograph (PV-LGC) an upper limit of 2 ppm at 22 km was determined (Oyama et al., 1980). In the cloud region, von Zahn et al. (1983) assume a mixing ratio of around 1 ppm. The most recent measurements of SOIR on board VEX indicate that the $H_2S$ mixing ratio decreases from 70 ppb at the cloud base at 47 km to less than 23 ppb at the cloud top (Krasnopolsky, 2008). As no measurements have been conducted above the cloud top and a sulfuric species, mostly present in the clouds, is not believed to have a constant mixing ratio up to the homopause, (see Section 2.3), we estimated the $H_2S$ mixing ratio to be around 1 ppb at 100 km. This value is not supported by any measurements and is seen as an upper limit.

*Hydrogen chloride (HCl):*

For the mixing ratio of HCl, a value of 0.1 ppm, valid in the mesosphere, is given by de Pater and Lissauer (2001). This is consistent with the most recent measurements conducted by SOIR on board VEX, where values of 0.1 ± 0.03 ppm and 0.17 ± 0.03 ppm were obtained for orbits 136 and 247, respectively, in the altitude range of 70–75 km (Bertaux et al., 2007). Taylor et al. (2018) assume a mixing ratio of 0.5 ppm, however, no altitude is specified. Thus, the number density models of HCl were conducted with a mixing ratio of 0.1 ppm at 120 km.

*Carbon dioxide(CO2):*

The most recent $CO_2$ measurements were performed with the SOIR spectrometer on board the ESA Venus Express mission (Mahieux et al., 2012). Since $CO_2$ was chosen to form the basis for the total number density of the atmosphere of Venus at the homopause, no mixing ratios but the effectively measured number density given in Mahieux et al. (2012) was used. The values are summarised in Table 1.

*Sulfur dioxide (SO2):*

$SO_2$ is another sulfur compound with a high mixing ratio below the clouds of around 200 ppm (de Pater and Lissauer, 2001) or 150 ppm (von Zahn et al., 1983; Taylor et al., 2018), but decreases quickly inside the cloud region down to a value of approximately 0.1 ppm at 70 km, due to conversion from $SO_2$ to the dominant species $H_2SO_4$ (von Zahn et al., 1983). $SO_2$ was measured above the cloud tops by the ultraviolet spectrometer SPICAV on board the ESA Venus Express, resulting in a mixing ratio of 0.1–0.2 ppm (Marcq et al., 2013). According to Krasnopolsky (2010), the mixing ratio stays constant up to around 110 km, before it decreases to around 60 ppb at 130 km. Thus, in this paper, a mixing ratio of 0.1 ppm at 100 km has been used.

*Carbonyl sulfide (COS):*

In the lower atmosphere, de Pater and Lissauer (2001) and Taylor et al. (2018) assume a COS mixing ratio of 4 ppm, whereas Hoffman et al. (1980a) rather suggest an upper limit of 3 ppm above 22 km, based on the data from the Pioneer Venus Mass Spectrometer. Measurements above the clouds were conducted with SOIR on board the ESA Venus Express mission, and mixing ratios of approximately 14 ppb at 64 km and 2 ppb at 70 km were reported (Krasnopolsky, 2008). No measurements were conducted above, hence, a mixing ratio of around 1 ppb at 100 km was estimated. This value is not supported by any measurements and is seen as an upper limit.

*Sulfuric acid (H2SO4):*

$H_2SO_4$ is the dominant species inside the clouds of Venus (Donahue and Russel, 1997). According to de Pater and Lissauer (2001), the mixing ratio of $H_2SO_4$ lies in the range of 1–2.5 ppm, however, these values probably correspond to the lower atmosphere. According to Krasnopolsky (2015), the production rate of $H_2SO_4$ decreases steadily above 66 km, with the mixing ratio having a peak of 8.5 ppm at 62 km. Above the cloud top, Krasnopolsky (2011) obtained a $H_2SO_2$ vapour mixing ratio of $10^{-12}$ at 70 and 110 km with a minimum of only $3 \cdot 10^{-18}$ at 88 km. However, Krasnopolsky (2011) mentions the large deviation between models. Zhang et al. (2010) developed another model according to which the $H_2SO_4$ mixing ratio at 100 km reaches a value of 0.1–1 ppb. According to Zhang et al. (2010), the results obtained are inconsistent with previous model results, however, they agree with recent observations by VEX. In this paper the upper limit given by Zhang et al. (2010) of 1 ppb at 100 km has been used.

### 2.4.2. Abundances of hot components

While thermal components have temperatures consistent with the atmospheric temperatures around them, hot components have much higher temperatures and therefore larger velocities. Hot components mainly get produced through dissociative recombination, i.e., the neutralisation of a positively charged molecule by the capture of an electron. In the atmosphere of Venus, the most dominant hot species are hydrogen, oxygen, nitrogen and carbon. Their concentrations are discussed in the following section and are summarised in Table 4.

*Hot hydrogen (H):*

A hot hydrogen number density of $n_H = 1.3 \cdot 10^9$ m$^{-3}$ at 255 km was derived from Lyman-$\alpha$ observations by measurements of the Mariner 5 mission with a corresponding temperature of 1020 K (Keating et al., 1985). Hot Hydrogen was also measured by SPICAV on board the ESA Venus Express mission, and a number density of $n_H = 2.5 \cdot 10^9$ m$^{-3}$ was derived for the dayside (Chaufray et al., 2012). In this paper, the values from Keating et al. (1985) were used as they also proposed a temperature together with the number density.

*Hot carbon (C):*

Hot carbon was also detected by the PV-OUVS, a value of $n_C = 1.0 \cdot 10^9$ m$^{-3}$ at 250 km was measured, together with a temperature of 4000 K (Keating et al., 1985).

*Hot nitrogen (N):*

From the data obtained by the PV-OUVS, a hot nitrogen component with a number density of $n_N = 1.0 \cdot 10^{10}$ m$^{-3}$ at 250 km was derived together with a temperature of 5500 K (Keating et al., 1985).

*Hot oxygen (O):*

For the number density of hot oxygen, the value used by Gunell et al.

**Table 4**
Used abundances of hot components on the dayside. No error estimates were given in the literature.

| Species | Number density [m$^{-3}$] | Altitude [km] | Temperature [K] | local time | Refrences |
|---|---|---|---|---|---|
| H | $1.3 \cdot 10^9$ | 255 | 1020 | dayside | [1],[2] |
| C | $1.0 \cdot 10^9$ | 250 | 4000 | not available | [1] |
| N | $1.0 \cdot 10^{10}$ | 250 | 5500 | not available | [1] |
| O | $7.5 \cdot 10^{10}$ | 200 | 6400 | dayside | [3] |

[1]Keating et al. (1985), [2]Chaufray et al. (2012), [3]Gunell et al. (2005).

(2005) of $n_O = 7.5 \cdot 10^{10}$ m$^{-3}$ was adopted in this paper, together with the corresponding temperature of 6400 K at 250 km. The values were obtained by measurements of the PV-OUVS and are valid on the dayside (Nagy et al., 1981).

#### 2.4.3. Mass spectra

From the number density profiles, mass spectra at a given altitude were derived by inter- or extrapolation of the density profiles. They show, which species and how many particles a mass spectrometer would measure at a given altitude over a certain integration time. The basis for the performance of the mass spectrometer is an instrument that was developed for lunar research (Wurz et al., 2012). The integration time to derive a mass spectrum determines the amount of background, for which the main source is given by the internal noise of the instrument. The longer the integration time, the smaller the background. This noise also defines the sensitivity of the mass spectrometer, i.e. its threshold, which in this case was set to 1 particle per cm$^{-3}$ for a 1 s integration. Choosing a long integration time comes with the assumption that the particle densities were constant throughout the whole measuring cycle. For a satellite on a highly elliptical orbit it is therefore recommended to choose short integration times and then, to lower the detection threshold to the background level, to combine multiple integration periods. However, short integration times come with large data rates.

For the mass spectra, the isotopes of the species were considered as well. As a simplification, the same isotopic ratios as on Earth were chosen. Firstly, because many of the simulated species have not been measured yet or their isotopic ratios have not been determined so far. Secondly, because several measured ratios are similar to the ones given on Earth, as for example the ratio $^{38}Ar/^{36}Ar$ with a value of $0.18 \pm 0.02$ on Venus, measured by the Pioneer Venus sounder probe neutral mass spectrometer, and 0.187 on Earth (Hoffman et al., 1980b). There are, however, a few isotopic ratios which show a larger deviation from the values found on Earth. One of them is the ratio between deuterium and hydrogen with D/H on Venus being approximately 150 times larger than on Earth (Paris and de Bergh, 1995).

## 3. Results and discussion

### 3.1. Density profiles

#### 3.1.1. Thermal species

For all simulated species, density profiles were calculated at the equator at noon, which corresponds to a solar zenith angle of 12 h local time. This method has been chosen because only for very few species a distinctive measurement concerning the mixing ratios with respect to local time is available. It would be a possible next step to extend the calculation by making a more detailed analysis on the densities with respect to latitudes and local times.

As mentioned in Section 2.1, the program is based on a Monte Carlo Simulation, and the density profiles are calculated by simulating the trajectory of a finite number of particles. However, the density decreases with the altitude, resulting in fewer particles at higher altitudes. This manifest itself in statistical uncertainties at large altitudes. In this paper, all simulations were conducted with a particle number of $10^6$. In several cases, especially when calculating mass spectra at higher altitudes, density values are required outside the computed altitude range. The density profiles have therefore been fitted by a function of the form

$$f(z) = \exp(a_1 + a_2 \cdot z), \tag{6}$$

where $z$ denotes the altitude and $a_1$, $a_2$ are the fitting parameters. The computed values are listed for all thermal species in Table 5. The errors resulting from the uncertainties of the abundances of the species in Venus' atmosphere outweigh the ones from the fitting.

Comparing Equation (6) with Equation (4), one can identifiy

**Table 5**
Fitting parameters from the linear regression of the density profiles.

| Species | $a_1$ | $a_2$ [km$^{-1}$] | Scale height [km] |
|---|---|---|---|
| Ar | 58.1655 | −0.199692 | 5.00771 |
| $CO_2$ | 73.6225 | −0.246976 | 3.70699 |
| COS | 61.2208 | −0.331964 | 3.01237 |
| CO | 59.8883 | −0.159495 | 6.26979 |
| C | 42.6991 | −0.0673318 | 14.8518 |
| $H_2O$ | 41.7274 | −0.0992705 | 10.0735 |
| $H_2SO_4$ | 83.0961 | −0.548353 | 1.82364 |
| $H_2S$ | 48.1267 | −0.201449 | 4.96404 |
| $H_2$ | 24.2176 | −0.0100817 | 99.1899 |
| HCl | 52.7876 | −0.207242 | 4.82528 |
| HF | 37.4708 | −0.113209 | 8.83322 |
| H | 26.7404 | −0.00280681 | 356.276 |
| He | 33.9373 | −0.0215026 | 46.5060 |
| Kr | 78.7967 | −0.464001 | 2.15517 |
| $N_2$ | 59.0051 | −0.153828 | 6.50077 |
| $NH_3$ | 34.7820 | −0.0967349 | 10.3375 |
| N | 44.5889 | −0.0794989 | 12.5788 |
| Ne | 45.7910 | −0.114484 | 8.73485 |
| $O_2$ | 54.6766 | −0.185894 | 5.37941 |
| O | 50.1651 | −0.0908983 | 11.0013 |
| $SO_2$ | 67.5318 | −0.349202 | 2.86367 |
| Xe | 106.852 | −0.737818 | 1.35535 |

$$H = -\frac{1}{a_2}. \tag{7}$$

The resulting scale heights are also shown in Table 5. One can also identify $\exp(a_1)$ with the number density at the surface of the planet. This method of fitting the data will deviate from the actual atmospheric parameters at lower altitudes, because the parameters obtained by Equation (6) are constant whereas the actual parameters are altitude dependent. The fitting implies a constant scale height, whereas the temperature gradient, as well as the change in the gravitational acceleration at different altitudes, make it very much altitude dependent. Fortunately, the effects of an altitude dependent scale height are negligible, since we restrict ourselves to altitudes much smaller than the radius of Venus for the thermal components.

In Fig. 1, the hydrogen, oxygen and nitrogen compounds as well as the noble gases are shown. The dashed segments of the species profiles clarify from where on the density has been extrapolated using the fitting function given in Equation (6). The thermal carbon component has been added to the oxygen compounds since it gets produced by dissociation of CO.

As can be seen in Fig. 1, the lighter the species the slower the decrease in density with altitude. Atomic hydrogen in Fig. 1a shows the smallest decrease, which is also related to the higher atmospheric temperatures at 255 km, from where the H density has been simulated, compared to 120 or 100 km.

The $CO_2$ density profile obtained with our model shown in Fig. 1b agrees only up to around 130 km with the measurements of SOIR on board the ESA Venus Express (Mahieux et al., 2012). The difference results from the temperature gradient. In our model, an initial temperature is assumed and taken to be constant at all altitudes, whereas in reality, the temperature reaches a minimum at around 120 km (Mahieux et al., 2015) and then starts to increase again. However, the derived density profile agrees with the measurements of the Pioneer Venus Bus Neutral Mass Spectrometer (PV-BNMS) up to the altitude of measurement of 180 km (Russel, 2012). But more important than reconstructing the measured density profile of $CO_2$ was obtaining the correct base to determine the total number density of the atmosphere, where mixing ratios are still valid. The decrease and following increase of the atmospheric temperature between 110 and 130 km lead to two inflection points in the slope of the $CO_2$ density (Mahieux et al., 2015) which cannot be reproduced by our model due to the constant temperature. The model of $CO_2$ would agree better with Mahieux et al. (2012) if we would have started the simulations above 130 km, however, as mentioned in

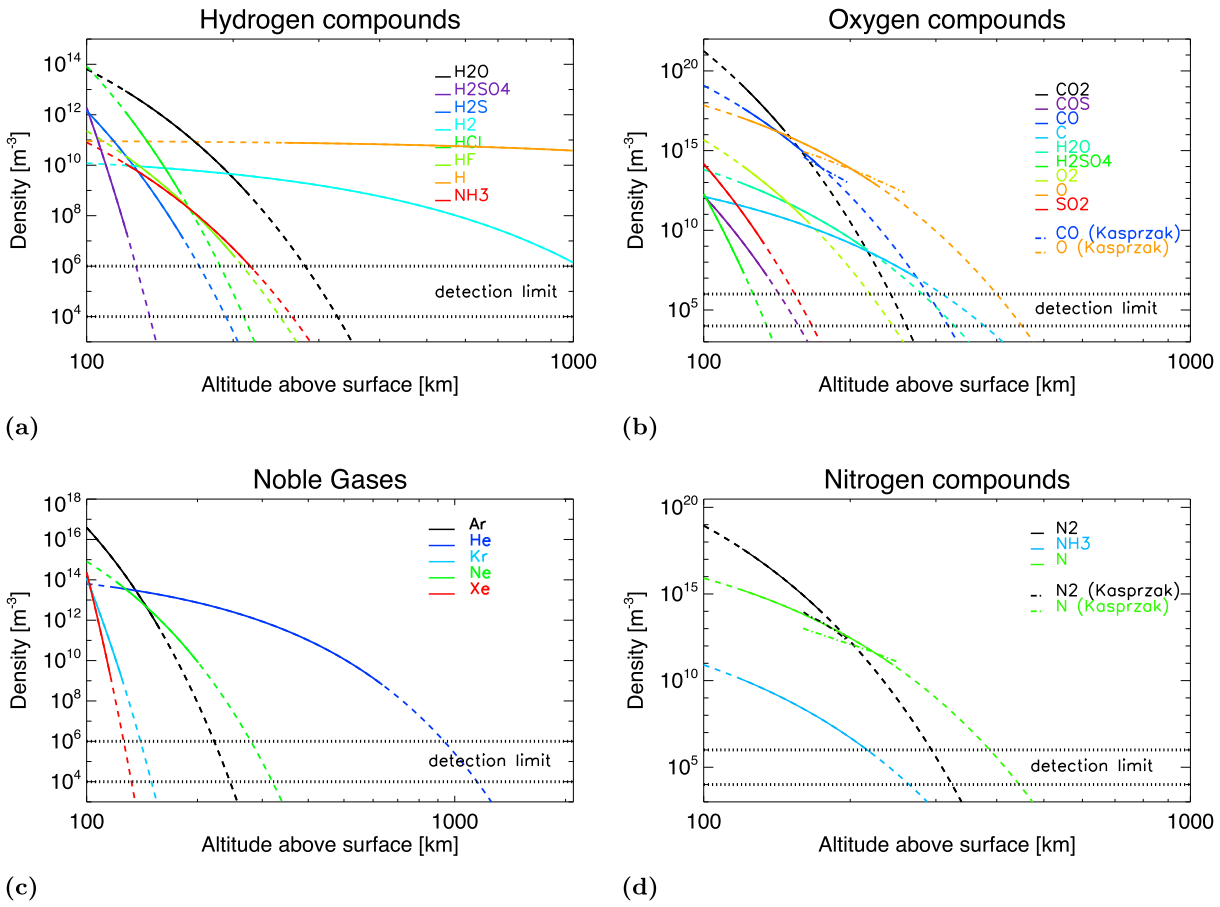


**Fig. 1.** Number density profiles of thermal hydrogen compounds (Fig. 1a), oxygen compounds (Fig. 1b), noble gases (Fig. 1c) and nitrogen compounds (Fig. 1d). The solid lines indicate the computed particle trajectories, whereas the dashed lines show from where on the density has been extrapolated. The dotted horizontal lines show the detection limit of the mass spectrometer, the upper and lower lines correspond to integration times of 1 s and $10^4$ s (≈ 2.8 h), respectively.

Section 2.3, mixing ratios cannot be considered to be constant up to this altitude.

In Fig. 1b and d, measurements obtained from the PV-ONMS (Kasprzak et al., 1980) for the species O, CO, N and $N_2$ are plotted. The measured data are in the same range as the modelled ones, however, they show a less steep slope. This probably results from the measurements containing both the hot and thermal components, whereas the plot only shows the thermal one. Including the hot component would make the density decrease more slowly and, hence, it would be in better agreement with the measurements. Unfortunately, there is no error given for the measurements. The hydrogen density will be analysed and compared to measurements further below in Section 3.1.2, together with the hot component. No detailed measurements of the sulfur compounds at these altitudes have been conducted so far.

For the noble gases, which are shown in Fig. 1c, the heavy noble gases xenon and krypton have a very small scale height, whereas helium, neon

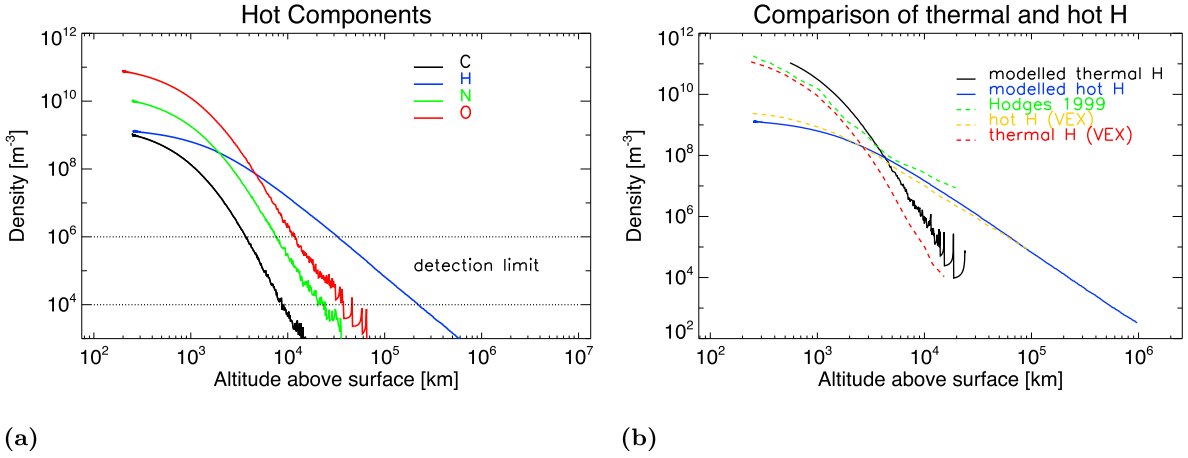


**Fig. 2.** Fig. 2a presents number density profiles of hot species. The dotted lines show the detection limit of the mass spectrometer, upper and lower lines corresponding to integration times of 1 s and $10^4$ s (≈ 2.8 h), respectively. In Fig. 2b, a comparison of the modelled thermal and hot hydrogen density profiles with the model derived by Hodges (1999) and the measurements made by SPICAV on board VEX are shown (Chaufray et al., 2012).

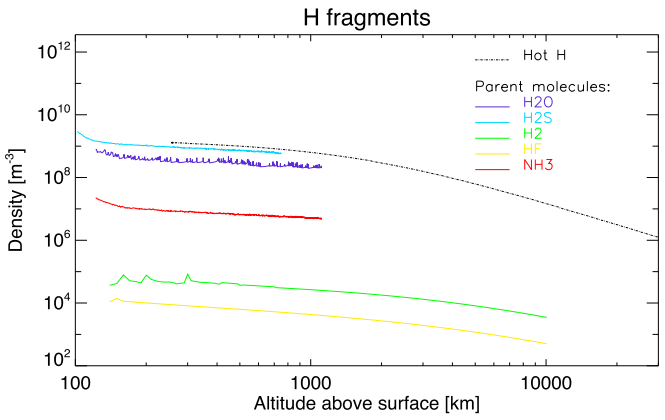


**Fig. 3.** Hydrogen fragments produced by photochemical dissociation of hydrogen compounds. The parent molecules are displayed in the legend.

and argon should be detectable up to at least 200 km, given a detection limit of one particle per $cm^{-3}$ for a 1 s integration, which is the common sensitivity for a mass spectrometer equivalent to the instrument developed for lunar research (Wurz et al., 2012) or NIM on board the JUICE mission (Vorburger et al., 2015a). The modelled He density has been compared to the measurements taken by the PV-BNMS and they agree fairly well, up to 700 km (Russel, 2012; Von Zahn et al., 1980). The detection of the heavy noble gases will be further discussed in Section 3.2.

### 3.1.2. Hot species

The hot atmospheric component is composed of high velocity particles, which received their energy mainly through dissociative recombination. The hot component is important to understand atmospheric escape. For the hot components in the exosphere, no fitting function of the form, as in Equation (6), could be applied. Even though the hot components were simulated in the same way as the thermal ones, with the difference lying in their higher initial temperatures and their origin somewhere along the trajectory of the parent molecule, the decay with altitude is no longer a simple exponential function. However, the higher temperature is also the reason for a much slower decay of their density, letting the particles reach much higher altitudes. Instead of a fitting function a simple logarithmic interpolation could therefore be used to obtain the required density values. The density profiles of the hot species are summarised in Fig. 2a.

The modelled hot hydrogen and oxygen density profiles compare well with the profiles obtained by Gunell et al. (2005), who modelled the hot hydrogen density by fitting the exospheric densities calculated by Rodriguez et al. (1984) and extrapolated their data to higher altitudes using a Chamberlain exosphere (Chamberlain and Hunten, 1987). In Fig. 2b, the thermal and hot hydrogen density profiles from our model (solid lines) were compared to the model obtained by Hodges (1999) and the measurements made by SPICAV on board the ESA Venus Express (dashed lines) (Chaufray et al., 2012) and it is clear that they agree well. Fig. 2b also shows that hot hydrogen should be measurable up to around 30'000 km, assuming a 1 s integration. Since we started with an initial value of thermal hydrogen lying above the one measured by VEX, our modelled profile (black curve) is above the one given by Chaufray et al. (2012) (red curve). But the two curves show the same behaviour in the decrease of the density with the altitude. The black curve representing the thermal hydrogen trajectory gets more and more noisy with the altitude, which again is a consequence of statistical uncertainties resulting from a finite number of simulated particles.

### 3.1.3. Photochemical dissociation

In Fig. 3 the hot hydrogen fragments produced by photochemical dissociation of the parent molecules $H_2O$, $H_2S$, $H_2$, HF and $NH_3$ are summarised. The black, dashed curve shows the hot hydrogen density profile obtained by the direct simulation of the hot hydrogen species, with initial values retrieved from Keating et al. (1985), also shown by the blue line in Fig. 2b. As one can see, the hydrogen fragment densities do not exceed the density obtained by the hot H model, which is good seeing that otherwise the number densities of the parent molecules or their photochemical dissociation rates would have been overestimated in our model. The summation of all hydrogen densities from photochemical dissociation is, furthermore, in the same range as the hot hydrogen density shown by the black curve. Taking into account that Fig. 3 compares the hot hydrogen densities obtained by two different approaches and yields a similar result, is a confirmation that the method for computing photochemical dissociation and our model in general is accurate.

But once again, choosing the initial altitude is critical because it has major effects on the photochemical dissociation, since it depends on the atmospheric temperature of the parent molecule, which, according to measurements of Mahieux et al. (2012), shows significant changes in the region between 100 and 130 km. Simulating the densities from 130 km on leads to far fewer fragments than completing the same computation at 120 km would. The fragments shown in Fig. 3 are therefore only the ones produced above the initial altitude. It is possible that more fragments were produced at lower altitudes, which can travel further up and result in a higher total photochemical dissociation density than shown in Fig. 3.

Photochemical dissociation of molecules is a key process for

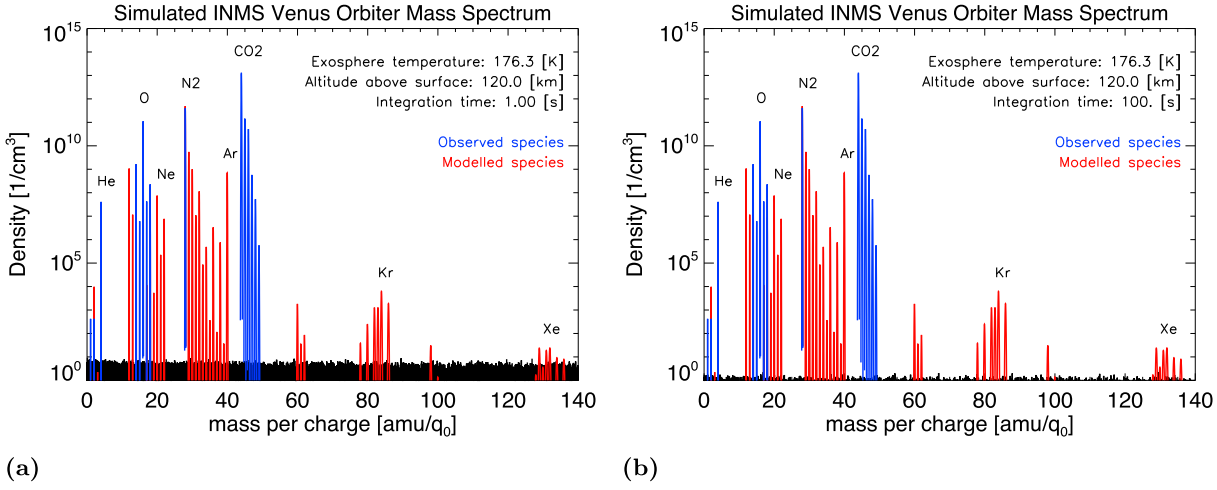


**Fig. 4.** Mass spectra of thermal components at 120 km altitude with an integration time of 1 s (Figs. 4a) and 100 s (Fig. 4b), respectively.

atmospheric escape, since it can provide the fragments with high enough energies to escape the gravitational field of the planet. According to Bertaux et al. (2007), the solar ultraviolet radiation breaks down the hydrogen-bearing molecules in the altitude range between 80 and 120 km, hence, the escape rate of hydrogen and consequently the planet's atmosphere evolution depends strongly on the abundance of these molecules in said altitude range.

### 3.2. Mass spectra

In Fig. 4 two mass spectra at 120 km are shown, assuming a performance of an instrument that was developed for lunar research (Wurz et al., 2012), with an integration time of 1 s and 100 s, respectively. The difference in the background, due to the integration times, is clearly visible. Signals with the colour blue indicate that the modelled number density agrees with available observational data, whereas red was chosen for the species which were not yet measured at all or with an accuracy which needs to be refined. The noble gases and few other species are indicated in the spectra for better orientation.

When having a closer look at Fig. 4a, one can see that the heavy noble gas xenon with a chemical mass of 131.298 u is hardly detectable by the mass spectrometer at this short integration time, with a signal-to-noise ratio (S/N) of about 3. Whereas with an integration time of 100 s, the Xe signal is visible in Fig. 4b with S/N ≈ 30.

Choosing the appropriate integration time depends on the satellite's orbit. A future Venus mission would likely have a similar orbit as the ESA Venus Express satellite, which arrived at Venus in 2006. For eight years, it had an elliptical 24-h orbit with distances in the periapsis and apoapsis of around 200 km and 66'000 km, respectively. After an aerobraking operation in 2014, the periapsis was lowered to around 130 km for approximately one month, and afterwards raised again to 460 km (ESA, 2014). A strongly elliptical orbit includes a high velocity of the satellite near periapsis. To observe the full dynamic range of the density profiles, short integration times are therefore recommended around closest approach. To reduce background, several of these short integration time spectra need to be accumulated afterwards during data processing on ground. 1 s spectra would be preferably recorded along the entire orbit, however, will increase the produced data volume significantly.

Since one of the major goals of future Venus missions, such as EnVision (Ghail et al., 2018), is to reconstruct the evolution of the planet, a measurement of the abundances of the noble gases is essential. The satellite therefore needs to reach an altitude low enough where the particle densities of the heavy noble gases lie above the sensitivity level of the mass spectrometer, which is 1 $cm^{-3}$ for a 1 s integration. Unfortunately, a 1 s spectrum cannot detect xenon around 130 km. An integration of 100 s would lower the detection limit to 0.1 $cm^{-3}$ and allow for the xenon detection, however, this would require a more circular orbit around Venus. A circular orbit at 130 km is not realistic, the dense atmosphere would slow down the satellite. For comparison, 50 s after closest approach, VEX already reached approximately 138 km. The lowest altitude allowing for the detection of Xe with a 1 s integration is around 123 km, with S/N ≈ 2–3. However, an orbit with low exentricity, e.g. periapsis and apoapsis at 130 km and 1000 km, respecitvely, could allow for the measurements.

To detect the noble gas components xenon, a closest approach distance of 120 km or less is recommended. To reach even lower altitudes would be better, if the spacecraft allows for that, taking into account that the upper limits for the Xe and also Kr mixing ratios have been used to

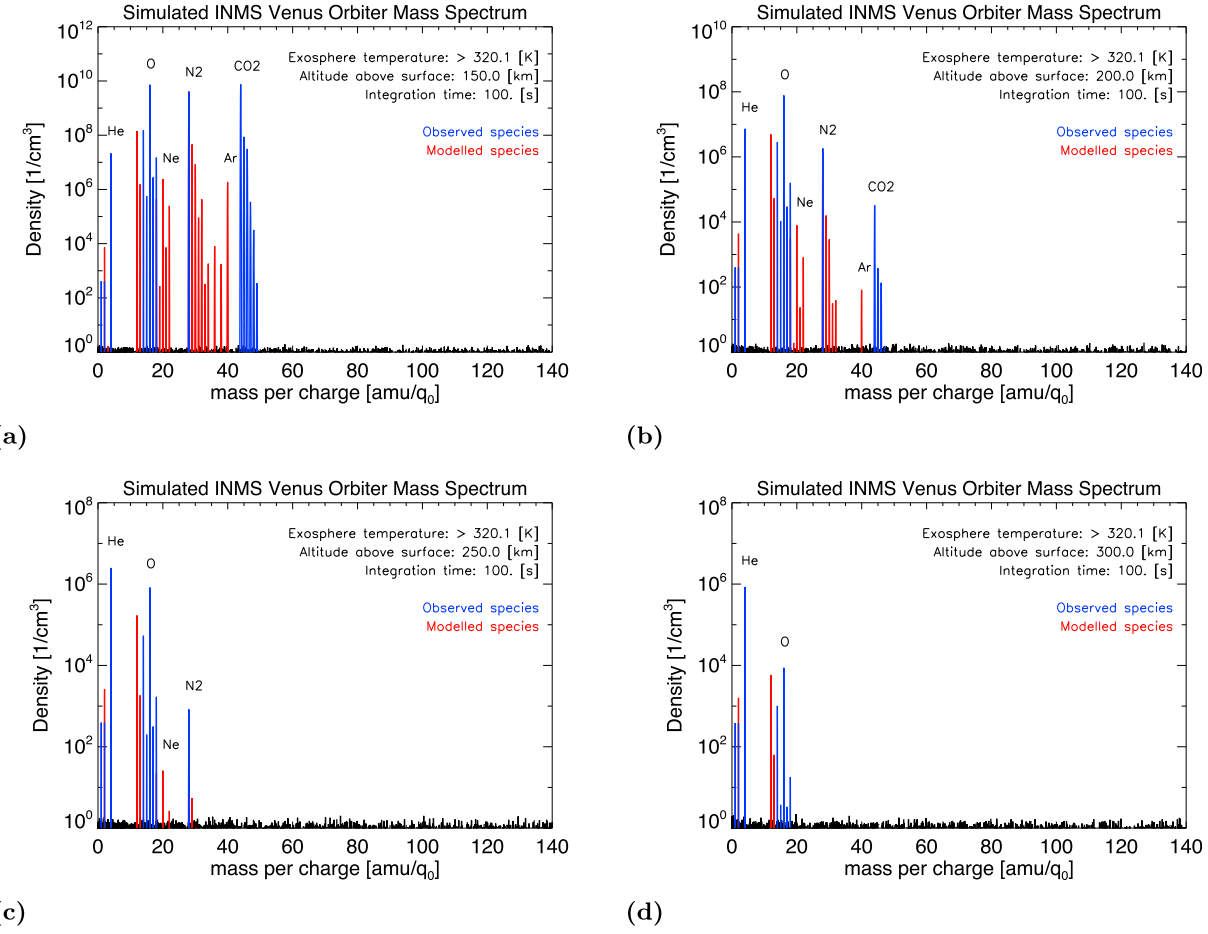


**Fig. 5.** Mass spectra of thermal components at altitudes of 150 km (Figs. 5a), 200 km (Figs. 5b), 250 km (Figs. 5c) and 300 km (Fig. 5d) with an integration time of 100 s.

compute the mass spectra and the uncertainty in their abundances is one order of magnitude (Chassefière et al., 2012). For the detection of krypton, our mass spectra predict a minimum distance of around 135 km.

Similar to VEX, the proposed EnVision mission of ESA will perform a 6 month-long aerobraking operation after an orbit insertion and periapse walk-down to achieve a 259 km circular orbit (Ghail et al., 2018). To achieve the circular orbit, the spacecraft first needs to slow down by firing its thrusters in opposite flying direction when it is in the apoapsis. This will lower the periapsis, e.g. VEX reached an altitude of only 130 km, and this could allow for measurements of heavy noble gases. However, a closest approach lower than 130 km should be considered. The mass spectrometric measurements will not be jeopardized by the thrusters since they will be turned off during closest approach. During atmospheric entry a heat shield will be required to protect the instruments. The atmosphere around periapsis will then already be dense enough to further slow down the satellite and lower the apoapsis. When the apoapsis will reach 259 km, the satellite needs to fire its thrusters to again bring the periapsis to the same altitude, leading to a circular orbit. No measurements need to be conducted during this second thrusting operation.

During atmospheric entry not only the heat but also the pressure are problematic, in particular when working with a mass spectrometer. A mass spectrometer working with conventional filaments requires a pressure $\leq 10^{-8}$ bar. At 120 km, however, given a density of around $10^{19}$ $m^{-3}$ and a temperature of 176 K, the pressure will be around $10^{-7}$ bar (assuming ideal gases). The mass spectrometer therefore needs to be suitably designed to survive such conditions. It might even be considered to use two different mass spectrometer, one for the lower and one for the higher atmosphere.

In Fig. 5, a selection of calculated mass spectra at different altitudes are shown, the integration time is specified in the legend of each plot. The higher the altitude, the harder to detect heavy species, leaving mostly hydrogen, helium and oxygen at 300 km altitude, as can be seen in Fig. 5d.

Thermal components are dominant in the atmosphere up to around 2800 km, where the number density of the thermal hydrogen component drops below the number density of the hot hydrogen component. The hot hydrogen component is measurable up to around 30′000 km (see Fig. 2b), assuming a sensitivity level of 1 $cm^{-3}$ for a 1 s integration.

In addition to the thermal species, a mass spectrometer should also measure the hot components, and the modelled spectra at four different altitudes, are shown in Fig. 6. From the measured density profiles of the hot components their atmospheric loss can be derived. The atmosphere between 300 and 5000 km is dominated by the hot oxygen component, and hydrogen dominates above. The less abundant hot species carbon and nitrogen should be measurable up to around 3600 and 7500 km, respectively, providing an integration time of 1 s and reducing background.

In addition to future Venus missions, the Jupiter Icy Moons Explorer (JUICE) mission of ESA with a launch date of June 2022 will make subsequent flybys of Earth, Venus and Mars (Gastaldello, 2016). For the Venus flyby, the closest approach is planned at a distance of 9535 km in October 2023. During this flyby the NIM/PEP mass spectrometer on board JUICE, designed to explore the atmospheric composition of Jupiter and its icy moons, could measure the hot hydrogen and oxygen components. According to Fig. 6d this should be possible at least around closest

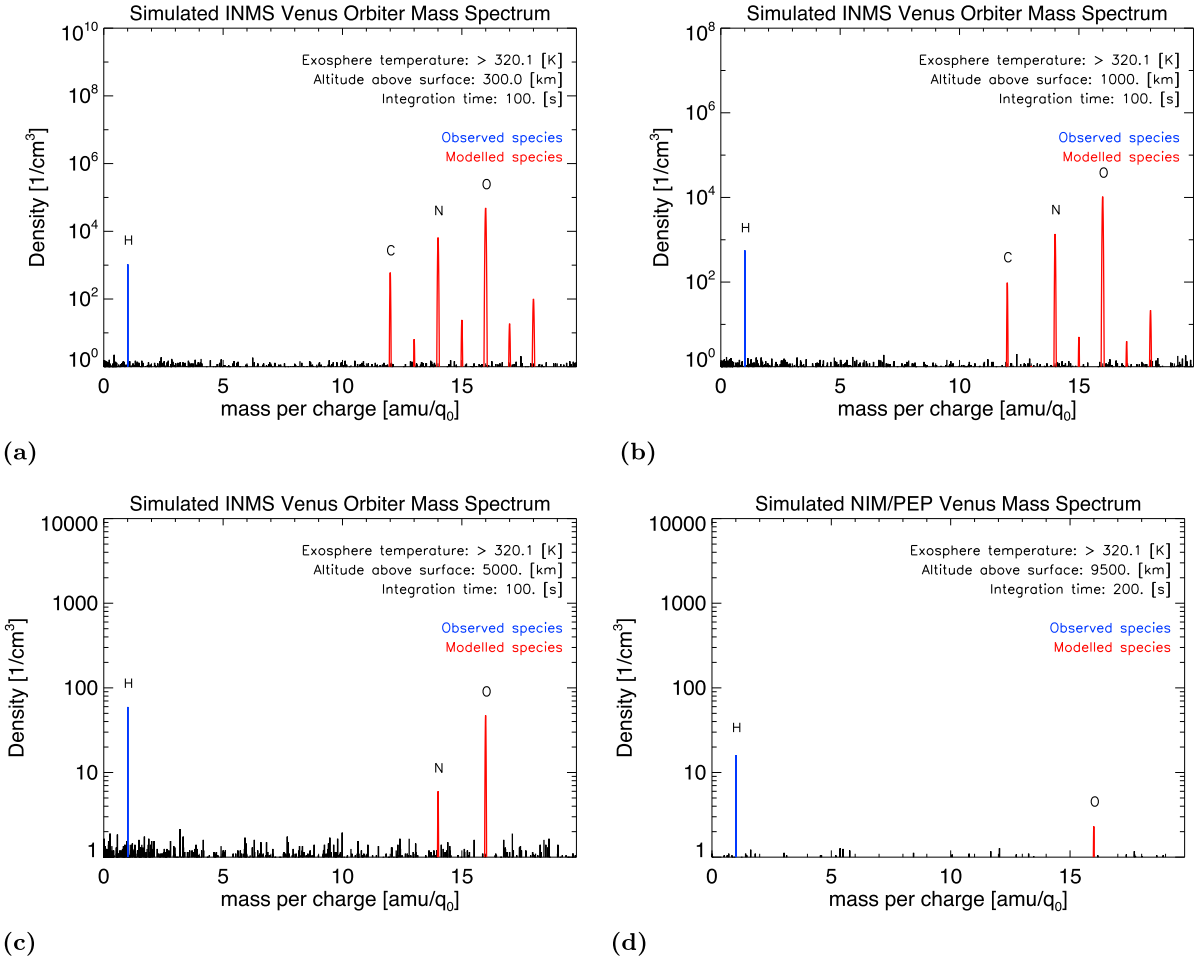


**Fig. 6.** Mass spectra of hot components at altitudes of 300 km (Figs. 6a), 1000 km (Figs. 6b), 5000 km (Figs. 6c) and 9500 km (Fig. 6d). All spectra correspond to an integration time of 100 s except for spectrum 6d which corresponds to an integration time of 200 s.

approach, but even if NIM/PEP would not measure anything this would still give us valuable information on the escape processes. This proposed measurement bears no risk for the mass spectrometer at all, since the distance to the planet is vast and there are no additional operations required.

Due to JUICE's trajectory not being an orbit but a flyby and since hot species have a much larger scale height than the thermal ones, the change in the particle densities along the trajectory are not as significant as for example along the elliptical orbit of VEX. Therefore, longer integration can be pursued. Around closest approach, an integration time of 200 s should be sufficient, seeing that 100 s after closest approach, the satellite should reach an altitude of 9551 km, only 16 km higher than at closest approach. Up to an altitude of approximately 20'000 km, which should be reached around 2 h after closest approach, integration times of 200 s are recommended. From there on it is proposed to accumulate at least two of the spectra to obtain spectra corresponding to 400 s. At 30'000 km, the particle density reaches the instruments' detection limit of 1 particle per $cm^{-3}$ for a 1 s integration.

In Fig. 6d, the corresponding calculated mass spectra at 9500 km is shown with an integration time of 200 s. At around 11'000 km, the hot oxygen density should have reached the detection limit of the mass spectrometer for a 1 s integration. At this distance, hot hydrogen should have decreased to a density of around 10 particles per $cm^3$.

## 4. Conclusion

We computed density profiles of several thermal and hot species in the upper atmosphere of Venus using an exospheric model. Wherever possible, the profiles were compared to existing measurements and previous models. The comparable profiles assort well with those measurements and models. From the profiles we derived mass spectra at several altitudes. Our calculations show that the heavy noble gases xenon and krypton might be detectable. The orbit discussion showed that an aerobraking operation is necessary to reach a low enough altitude and therefore, the EnVision mission planned by ESA offers the perfect opportunity to conduct those fundamental measurements. We have also shown that JUICE might be able to measure the hot oxygen and hydrogen densities during its Venus flyby which would provide us with information about the escape processes. This way, the two missions could complement each other so that in the future our models could get even more accurate.

The last in-situ measurements in Venus' atmosphere are more than 30 years old and many new questions have arisen and also some old ones still need answering. A new mission to explore our neighbour could be able to answer some of them and a measurement of the heavy noble gases would not only widen our understanding of the evolution of Venus, but that of Earth too. The EnVision mission carrying a mass spectrometer is therefore the perfect candidate for a space exploration in the near future.

## Acknowledgements

This work is funded by the Swiss National Science Foundation (SNF).

## Appendix A. Photochemical dissociation

Photochemical dissociation of molecules in the atmosphere of Venus is dominated by solar photons. The theoretical photochemical dissociation time is therefore related to the photoionisation. According to Huebner et al. (1991), photochemical dissociation of a molecule $AB$ by a photon of energy $h\nu$ can take place over the following reactions:

$$AB + h\nu \rightarrow A + B \rightarrow A + B^+ + e^-. \tag{A.1}$$

In Huebner et al. (1991) the solar ionisation rates are given together with the excess energies and rate coefficients for all species and all reactions that may take place involving photons. The solar photoionisation rate is given by the reaction

$$AB + h\nu \rightarrow AB^+ + e^-, \tag{A.2}$$

whereas the rate coefficients of all other reactions define the photochemical dissociation time.

Atomic species do not undergo the photochemical dissociation process, however, they can interact with photons too, mainly by the reaction

$$A + h\nu \rightarrow A^+ + e^-. \tag{A.3}$$

The photoionisation rate is given by the rate coefficient of this process.

Since the solar photoionisation rates $\eta$ given in Huebner et al. (1991) correspond to $R_0 = 1$ AU, a scaling to the distance between the Sun and Venus, $R$, has to be applied.

$$\eta_{\text{Venus}} = \eta_{1\text{AU}} \cdot \left(\frac{R_0}{R}\right)^2, \tag{A.4}$$

where $R$ denotes the medium distance between Venus an the Sun, given by $R \approx 0.723$ AU (Williams, 2016).

## References

Anderson, D.E., 1976. The Mariner 5 ultraviolet photometer experiment - analysis of hydrogen Lyman alpha data. J. Geophys. Res. 81, 1213–1216. http://adsabs.harvard.edu/abs/1976JGR...81.1213A.

Bailey, J., 2013. Mariner 2 and its legacy: 50 Years on 78 (october 1960). http://arxiv.org/abs/1302.3675.

Basilevsky, A.T., Ivanov, M.A., Head, J.W., Aittola, M., Raitala, J., 2007. Landing on venus: past and future. Planet. Space Sci. 55 (14), 2097–2112.

Bertaux, J.L., Vandaele, A.C., Korablev, O., Villard, E., Fedorova, A., Fussen, D., Quémerais, E., Belyaev, D., Mahieux, A., Montmessin, F., Muller, C., Neefs, E., Nevejans, D., Wilquet, V., Dubois, J.P., Hauchecorne, A., Stepanov, A., Vinogradov, I., Rodin, A., Nevejans, D., Montmessin, F., Fedorova, A., Cabane, M., Chassefière, E., Chaufray, J.Y., Dimarellis, E., Dubois, J.P., Hauchecorne, A., Leblanc, F., Lefèvre, F., Rannou, P., Quémerais, E., Villard, E., Fussen, D., Muller, C., Neefs, E., Van Ransbeeck, E., Wilquet, V., Stepanov, A., Vinogradov, I., Zasova, L., Forget, F., Lebonnois, S., Titov, D., Rafkin, S., Durry, G., Gérard, J.C., Sandel, B., 2007. A warm layer in Venus' cryosphere and high-altitude measurements of HF, HCl, H2O and HDO. Nature 450 (7170), 646–649.

Bindschadler, D.L., 1995. Magellan: a new view of Venus' geology and geophysics. Rev. Geophys. 33 (1 S), 459–467.

Brecht, A.S., Bougher, S.W., Gérard, J.C., Soret, L., 2012. Atomic oxygen distributions in the Venus thermosphere: comparisons between Venus Express observations and global model simulations. Icarus 217 (2), 759–766.
Chamberlain, J.W., Hunten, D.M., 1987. Theory of Planetary Atmospheres, vol. 36. http://adsabs.harvard.edu/abs/1987tpaa.book…C.
Chassefière, E., Wieler, R., Marty, B., Leblanc, F., 2012. The evolution of Venus: present state of knowledge and future exploration. Planet. Space Sci. 63–64, 15–23.
Chaufray, J.Y., Bertaux, J.L., Quémerais, E., Villard, E., Leblanc, F., 2012. Hydrogen density in the dayside venusian exosphere derived from Lyman-$\alpha$ observations by SPICAV on Venus Express. Icarus 217 (2), 767–778. https://doi.org/10.1016/j.icarus.2011.09.027.
Colin, L., Hall, C.F., 1977. The pioneer venus program. Space Sci. Rev. 20 (3), 283–306.
Connes, P., Connes, J., Benedict, W.S., Kaplan, L.D., 1967. Traces of HCl and HF in the atmosphere of Venus, vol. 147, pp. 1230–1237.
Cottini, V., Ignatiev, N.I., Piccioni, G., Drossart, P., Grassi, D., Markiewicz, W.J., 2012. Water vapor near the cloud tops of Venus from Venus Express/VIRTIS dayside data. Icarus 217 (2), 561–569.
de Pater, I., Lissauer, J., 2001. Planetary Sciences. Planetary Sciences. http://adsabs.harvard.edu/abs/2001plsc.book…D.
Donahue, T.M., Arbor, A., Hoffman, J.H., Hodges, R.R., 1981. Krypton and Xenon in the Atmosphere of Venus, Department of Atmospheric and Oceanic Science, University of Michigan, Department of Physics. University of Texas, Dallas, Richardson, pp. 513–516. Texas 75080 spectrometer are reported. An upper limit to most of t 8 (5).
Donahue, T.M., Russel, C.T., 1997. The Venus Atmosphere and Ionosphere and Their Interaction with the Solar Wind: an Overview.
ESA, 2014. Venus Express goes gently into the night. http://sci.esa.int/venus-express/55141-venus-express-goes-gently-into-the-night/.
Gastaldello, N., 2016. Preliminary Navigation Analysis for the Flyby Tour of ESA's JUICE Mission.
Gelman, G., Zolotukhin, B.G., Lamonov, V.I., 1979. An Analysis of the Chemical Composition of the Atmosphere of Venus on an AMS of the Venera-12 Using a Gas Chromatograph.
Gérard, J.C., Saglam, A., Piccioni, G., Drossart, P., Montmessin, F., Bertaux, J.L., 2009. Atomic oxygen distribution in the Venus mesosphere from observations of O2 infrared airglow by VIRTIS-Venus Express. Icarus 199 (2), 264–272.
Ghail, R., Bruzzone, L., Mason, P., Wilson, C., Rosenblatt, P., 2018. EnVision: understanding why our most Earth-like neighbour is so different. https://arxiv.org/pdf/1703.09010.pdf.
Gilli, G., López-Valverde, M.A., Peralta, J., Bougher, S., Brecht, A., Drossart, P., Piccioni, G., 2015. Carbon monoxide and temperature in the upper atmosphere of Venus from VIRTIS/Venus Express non-LTE limb measurements. Icarus 248, 478–498.
Gunell, H., Holmström, M., Biernat, H.K., Erkaev, N.V., 2005. Planetary ENA imaging: venus and a comparison with Mars. Planet. Space Sci. 53 (4), 433–441.
Hedin, A.E., Niemann, H.B., Kasprzak, W.T., 1983. Global empirical model of the venus thermosphere. J. Geophys. Res. 88 (A1), 73–83. https://doi.org/10.1029/JA088iA01p00073.
Hodges, R.R., 1999. An exospheric perspective of isotopic fractionation of hydrogen on Venus. J. Geophys. Res.: Plan 104 (E4), 8463–8471.
Hoffman, J., Hodges, R., Donahue, T., McElroy, M.B., 1980a. Composition of the venus lower atmosphere from the pioneer venus mass spectrometer. J. Geophys. Res. 85 (80), 7882–7890. http://www.agu.org/pubs/crossref/1980/JA085iA13p07882.shtml.
Hoffman, J., Hodges, R., Donahue, T., McElroy, M.B., 1980b. Composition of the venus lower atmosphere from the pioneer venus mass spectrometer. J. Geophys. Res. 85 (80), 7882–7890. http://www.agu.org/pubs/crossref/1980/JA085iA13p07882.shtml.
Huebner, W.F., Keady, J.J., Lyon, S.P., 1991. Solar Photo Rates for Planetary Atmospheres and Atmospheric Pollutants, p. 293.
Istomin, V.G., Grechnev, K.V., Kotchnev, V.A., 1980. Mass spectrometer measurements of the composition of the lower atmosphere of venus. COSPAR Colloquia Series 20 (C), 215–218.
Kasprzak, W.T., Hedin, A.E., Niemann, H.B., Spencer, N.W., 1980. Atomic nitrogen in the upper atmosphere of Venus. Geophys. Res. Lett. 7 (1), 106–108.
Kasprzak, W.T., Keating, G.M., Hsu, N., Stewart, A.I.F., ColWell, W.B., Bougher, S.W., 1997. Solar activity behavior of the therrmosphere. http://adsabs.harvard.edu/abs/1997veii.conf…225K, 225.
Keating, G., 1980. Venus upper atmosphere structure. J. Geophys. 85 (80), 7941–7956. http://onlinelibrary.wiley.com/doi/10.1029/JA085iA13p07941/full.
Keating, G.M., Bertaux, J.L., Bougher, S.W., Cravens, T.E., Dickinson, R.E., Hedin, A.E., Krasnopolsky, V.A., Nagy, A.F., Nicholson, J.Y., Paxton, L.J., Zahn, U.V., 1985. Chapter IV models of venus neutral upper atmosphere: structure and composition. Adv. Space Res. 5 (11), 117–171.
Krasnopolsky, V., 2012. Observation of DCl and upper limit to NH3on Venus. Icarus 219 (1), 244–249.
Krasnopolsky, V.A., 2008. High-resolution spectroscopy of Venus: detection of OCS, upper limit to H2S, and latitudinal variations of CO and HF in the upper cloud layer. Icarus 197 (2), 377–385.
Krasnopolsky, V.A., 2010. Venus night airglow: ground-based detection of OH, observations of O2 emissions, and photochemical model. Icarus 207 (1), 17–27.
Krasnopolsky, V.A., 2011. Vertical profile of H2SO4vapor at 70-110km on Venus and some related problems. Icarus 215 (1), 197–203.
Krasnopolsky, V.A., 2015. Vertical profiles of H2O, H2SO4, and sulfuric acid concentration at 45-75 km on Venus. Icarus 252, 327–333.
Krasnopolsky, V.A., Gladstone, G.R., 2002. ¿Helium on Mars and venus: EUVE observations and modeling. Astron. Astrophys. 386 (1), 319–330.
Mahieux, A., Vandaele, A.C., Bougher, S.W., Drummond, R., Robert, S., Wilquet, V., Chamberlain, S., Piccialli, A., Montmessin, F., Tellmann, S., Pätzold, M., Häusler, B., Bertaux, J.L., 2015. Update of the Venus density and temperature profiles at high altitude measured by SOIR on board Venus Express. Planet. Space Sci. 113–114, 309–320.
Mahieux, A., Vandaele, A.C., Robert, S., Wilquet, V., Drummond, R., Montmessin, F., Bertaux, J.L., 2012. Densities and temperatures in the Venus mesosphere and lower thermosphere retrieved from SOIR on board Venus Express: carbon dioxide measurements at the Venus terminator. J. Geophys. Res.: Plan 117 (7).
Marcq, E., Bertaux, J.L., Montmessin, F., Belyaev, D., 2013. Variations of sulphur dioxide at the cloud top of Venus's dynamic atmosphere. Nat. Geosci. 6 (1), 25–28. https://doi.org/10.1038/ngeo1650.
Nagy, A.F., Cravens, T.E., Yee, J.H., Stewart, A.I., 1981. Hot oxygen atoms in the upper atmosphere of Venus. Geophys. Res. Lett. 8 (6), 629–632.
Niemann, H.B., Kasprzak, W.T., Hedin, A.E., Spencer, N.W., Hunten, D.M., 1980. Mass spectrometric measurements of the neutral gas composition of the thermosphere and exosphere of Venus. J. Geophys. Res. 85 (A13), 7817–7827.
Owen, T., Sagan, C., 1972. Minor constituents in planetary atmospheres: ultraviolet spectroscopy from the orbiting astronomical observatory. Icarus 16 (3), 557–568.
Oyama, V., Carle, G.C., Woeller, F., Pollack, J.B., Reynolds, R.T., Craig, R.A., 1980. Pioneer Venus gas chromatography of the lower atmosphere of Venus. J. Geophys. Res. 85 (80), 7891–7902.
Paris, D., de Bergh, C., 1995. Isotopic ratios in planetary atmospheres. Adv. Space Res.: Off. J. Comm. Space Res. (COSPAR) 15 (3), 427–440.
Rodriguez, J.M., Prather, M.J., McElroy, M.B., 1984. Hydrogen on venus: exospheric distribution and escape. Planet. Space Sci. 32 (10), 1235–1255.
Russel, C., 2012. Venus Aeronomy. Springer Netherlands. https://books.google.ch/books?id=IUzvCAAAQBAJ.
Surkov, Y.A., Andreichikov, B.M., Kalinkina, O.M., 1974. Composition and Structure of the Cloud Layer of Venus, pp. 673–678. http://adsabs.harvard.edu/abs/1974spre.conf…673S.
Svedhem, H., Titov, D., Taylor, F., Witasse, O., 2009. Venus express mission. J. Geophys. Res.: Plan 114 (5), 1–19.
Taguchi, M., Fukuhara, T., Futaguchi, M., Sato, M., Imamura, T., Mitsuyama, K., Nakamura, M., Ueno, M., Suzuki, M., Iwagami, N., Hashimoto, G.L., 2012. Characteristic features in Venus' nightside cloud-top temperature obtained by Akatsuki/LIR. Icarus 219 (1), 502–504. https://doi.org/10.1016/j.icarus.2012.01.024.
Taylor, F.W., 2014. The Scientific Exploration of Venus.
Taylor, F.W., Svedhem, H., Head, J.W., 2018. Venus: the Atmosphere, Climate, Surface, Interior and Near-Space Environment of an Earth-like Planet.
Vandaele, A.C., Chamberlain, S., Mahieux, A., Ristic, B., Robert, S., Thomas, I., Trompet, L., Wilquet, V., Belyaev, D., Fedorova, A., Korablev, O., Bertaux, J.L., 2016. Contribution from SOIR/VEX to the updated venus international reference atmosphere (VIRA). Adv. Space Res. 57 (1), 443–458.
Vandaele, A.C., Mahieux, A., Robert, S., Drummond, R., Wilquet, V., Bertaux, J.L., 2015. Carbon monoxide short term variability observed on Venus with SOIR/VEX. Planet. Space Sci. 113–114, 237–255. https://doi.org/10.1016/j.pss.2014.12.012.
Von Zahn, U., Fricke, K., Hunten, D., Krankowsky, D., Mauersberger, K., Nier, A., 1980. The upper atmosphere of Venus during morning conditions. J. Geophys. Res. 85 (A13), 7829–7840. http://www.agu.org/pubs/crossref/1980/JA085iA13p07829.shtml.
von Zahn, U., Kumar, S., Niemann, H., Prinn, R., 1983. Composition of the venus atmosphere. http://adsabs.harvard.edu/abs/1983vens.book…299V.
von Zahn, U., Moroz, V.I., 1985. Composition of the Venus atmosphere below 100 km altitude. Adv. Space Res. 5 (11), 173–177.
Vorburger, A., Wurz, P., Galli, A., Mousis, O., Barabash, S., Lammer, H., 2015a. Modelling of NIM/PEP/JUICE Measurements of Callisto's Ice-Sputtered Exosphere EPSC2015-7, pp. 1–2.
Vorburger, A., Wurz, P., Lammer, H., Barabash, S., Mousis, O., 2015b. Monte-Carlo simulation of Callisto's exosphere. Icarus 262, 14–29.
Williams, D.R., 2016. Venus fact sheet. https://nssdc.gsfc.nasa.gov/planetary/factsheet/venusfact.html.
Wurz, P., Abplanalp, D., Tulej, M., Lammer, H., 2012. A neutral gas mass spectrometer for the investigation of lunar volatiles. In: Planetary and Space Science, vol. 74, pp. 264–269.
Wurz, P., Lammer, H., 2003. Monte-Carlo simulation of Mercury's exosphere. Icarus 164 (1), 1–13.
Wurz, P., Rohner, U., Whitby, J.A., Kolb, C., Lammer, H., Dobnikar, P., Martín-Fernández, J.A., 2007. The lunar exosphere: the sputtering contribution. Icarus 191 (2), 486–496.
Young, A.T., 1977. An improved Venus cloud model. Icarus 32 (1), 1–26.
Zhang, X., Liang, M.C., Montmessin, F., Bertaux, J.L., Parkinson, C., Yung, Y.L., 2010. Photolysis of sulphuric acid as the source of sulphur oxides in the mesosphere of Venus. Nat. Geosci. 3 (12), 834–837.